Experimental Characterization and Numerical Modelling of an Electric Vehicle Thermal Management System Integrating a Screw-Type e-Pump

Stefano Li Veli[1], Luca Romagnuolo[2], Valerio Di Cosmo[2], Emma Frosina[1*], Adolfo Senatore[2]

[1] *Department of Engineering, University of Sannio, Benevento, Italy*
[2] *Department of Industrial Engineering, University of Naples Federico II, Naples, Italy*

**E-mail: frosina@unisannio.it*

Abstract

Nowadays, the adoption of electric and hybrid-electric propulsion systems has become a common solution for the stringent decarbonization requirements. These technologies require advanced thermal management solutions capable of ensuring effective cooling of critical components while limiting energy consumption. Although centrifugal pumps are commonly used in cooling circuits, their performance can be affected by variable pressure losses and changing operating conditions, reducing flow-control accuracy. This work presents the experimental characterization, numerical modelling, and validation of a thermal management system for a high-performance electric vehicle, integrating a prototype screw-type positive-displacement e-pump. Tests were carried out on a dedicated test rig to hydraulically characterize the main circuit's components, including the electric motor and inverter, under different pump speeds and flow-rate distributions imposed by a needle-valve adjustment. The collected data were used to calibrate and validate a lumped-parameter model developed in Simcenter AMESim. The model accurately reproduced the measured pressure losses and the flow distribution across the different circuit branches, confirming the reliability of the numerical approach.

Keywords. Battery Electric Vehicle, Thermal Management System, Screw-type e-Pump, Experimental analysis and Numerical Validation

1. INTRODUCTION

In recent years, increasing attention has been paid to the environmental sustainability, with the aim of reducing pollution and, more specifically, CO_2 emissions. The transport sector has gained a prominent role and visibility in this context, although it is not the largest contributor [1]. However, this sector has historically shown some delay compared to others;

indeed, its emissions continued to increase until 2007, when the first micro-hybrid technologies, such as Start & Stop systems, began to spread. Emissions started to decrease more consistently only with the subsequent diffusion of hybrid vehicles, including full and mild hybrid electric vehicles, battery electric vehicles (BEVs), and fuel-cell electric vehicles (FCEVs) [2], [3].

The adoption of these new technologies, widely regarded as the most effective solutions to achieve environmental targets, has introduced new technological challenges. Among these, the thermal management of electrified powertrain components plays a crucial role. The main components of an electric vehicle (EV) powertrain, namely batteries, electric motors, inverters, and power conversion systems, operate within relatively narrow temperature ranges [4]. Exceeding these limits results in a significant reduction in performance, efficiency, and component lifetime, together with potential safety concerns. [4], [5].For these reasons, the Thermal Management System (TMS) of electric and hybrid powertrains represents a key subsystem in EVs. The development and optimization of this subsystem have a strong impact on performance improvement, driving range extension, and reliability enhancement[6].

Nowadays, conventional thermal management systems for EVs, rely on liquid cooling circuits driven by centrifugal pumps. This well-established configuration is generally adopted because of its relative simplicity and low costs [7]. Nevertheless, centrifugal pumps may show limitations in terms of efficiency and flow-rate regulation, especially when not operating in their optimal working ranges or within systems affected by variable pressure drops. Under these conditions, cooling performance could be affected, with a subsequent power consumption increase and overall efficiency decrease [8].

This work proposes an innovative TMS, specifically intended for high-performance EVs, which replaces the conventional centrifugal pump with an innovative positive displacement electrically driven pump (e-pump). The performance of this type of pump is generally less sensitive to the operating conditions of the system when compared to centrifugal ones [9], [10], [11]. In this way, greater operational flexibility can be achieved, enabling a more effective response to different working conditions. Moreover, the proposed pump may also enhance vehicle comfort by reducing noise emissions, an aspect that is becoming increasingly relevant in EVs due to their inherently lower overall noise levels.

The research activity described in this paper focused on the development and use of experimental test rigs for characterizing the main components of the thermal management system. It also addressed, as said, the implementation and integration of the positive displacement pump, the definition of possible system architectures based on this pumping technology, and the development of a lumped-parameter numerical model using the Simcenter AMESim® environment.

This work is part of a research project supported by the Italian Minister "Ministero delle imprese e del made in Italy", involving three Universities: Politecnico di Milano (PoliMI), CeSMA of University of Naples Federico II (UniNA), and University of Sannio (UniSannio) and the company Fluid-o-Tech srl, leader of the project. Preliminary results achieved by the authors were also presented in a previous publication [12].

2. EXPERIMENTAL ACTIVITIES

The aim of the experimental activity presented in this work was to perform a fluid-dynamic characterization of the main components cooled by an innovative TMS designed within the project, with particular focus on the electric motor and inverter. The experimental campaign was conducted at the laboratories of the University of Naples Federico II. Following the preliminary analysis and hydraulic tests of the individual components, a test rig was set up to measure pressure losses as a function of coolant flow rate, providing the data required for the simulation and calibration of the cooling circuit model. The resulting data were then processed and used to build a predictive numerical model.

The physical test-rig is outlined in Figure 1 and showed in Figure 2. A water-ethylene glycol (EG50W50) reservoir (1) feeds the e-pump under investigation (3). The pump speed is regulated via proprietary software. The coolant flow is then split into two branches serving the cooling circuits of the electric motor (9) and the inverter (10). A needle valve (7) is installed to regulate the flow rate distribution among the two branches, which is measured by two flow meters (5 – FM2, 6 – FM1). Downstream, two fan-coil units (12, 13), arranged in parallel, provide the heat-dissipation function of the circuit radiator. Three pairs of pressure and temperature sensors are located upstream of the inverter (8 – P1, T1), between the cooled components and the heat exchangers (11 – P2, T2), and downstream of the fan coil units (14 – P3, T3). An additional pressure sensor (4 – P0) is installed downstream of the pump. All the sensors installed in the circuit are listed in Table 1.

Table 1. Specifications of the sensors used in the experimental setup

ID	Variable	Type	Brand, Model	Range, Accuracy
FM1	Flowrate	Coriolis	Endress Proline 83F15	0 ÷ 6500 kg/h, ± 0.35%
FM2	Flowrate	Vortex	IFM SV5200	2-48 L/min, ±0.5%
P0,P1	Pressure	Transducer	Gesensing PMP1400	0 ÷ 4 bar, ± 0.15%
P2,P3	Pressure	Transducer	IFM PU5415	0 ÷ 6 bar, ± 0.5%
T1, T2, T3	Temperature	Thermocouple	Thermocouple K type	-200 ÷ 1100 °C, ± 1.5 °C

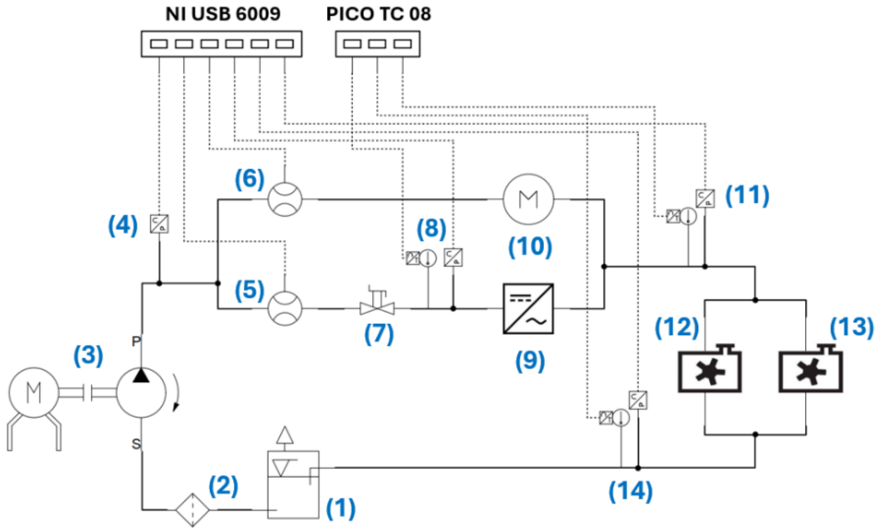

Figure 1. Schematic layout of the experimental test rig.

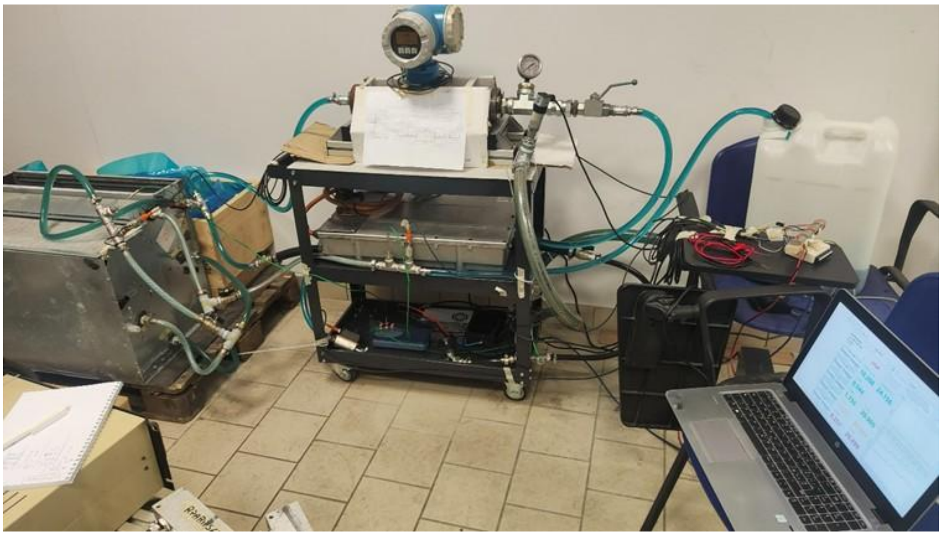

Figure 2. Photograph of the physical test rig

To physically assemble the circuit and connect components with different sizes and interfaces, several auxiliary components were used in addition to rubber hoses with nominal diameters of ½″, 1″, and 1¼″. These auxiliary components are listed in Figure 3, together with their locations in the circuit schematic.

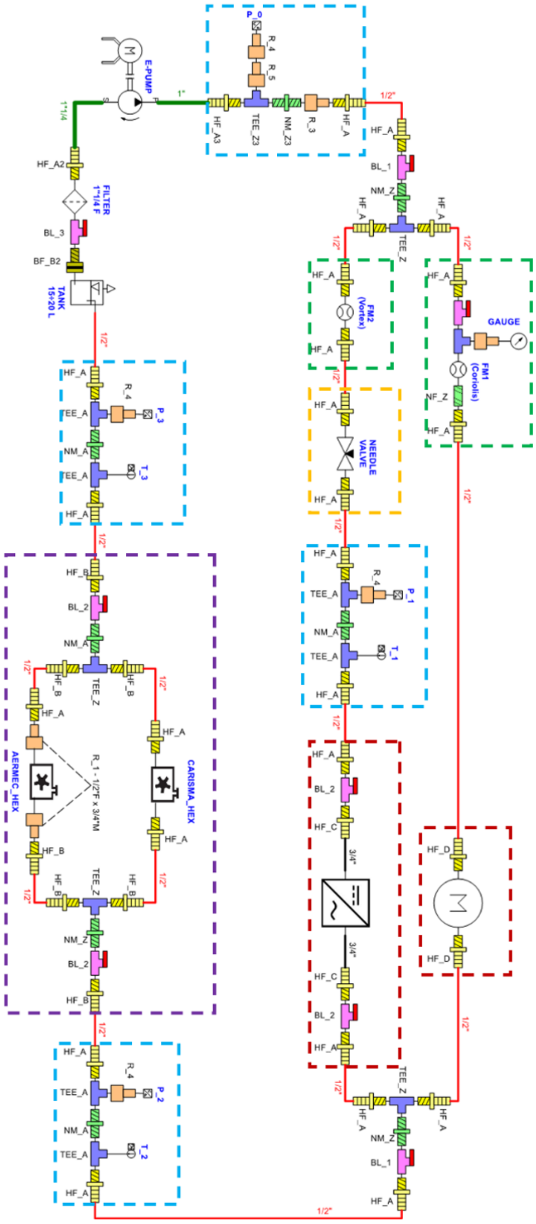

Symbol	Name	Description
	HF_A	Hose fitting, stainless steel, 1/2" x 12.7 mm
	HF_A2	Hose fitting, stainless steel, 1"1/4 x 31.8 mm
	HF_A3	Hose fitting, stainless steel, 1" x 25.4 mm
	HF_B	Hose fitting, brass, 1/2" x 15 mm
	HF_C	Hose fitting, brass, 1/2" x 20 mm
	R_1	Reducer, stainless steel, 1/2"F x 3/4"M
	R_2	Reducer, stainless steel, 1/2"F x 1"1/4 F
	R_3	Reducer, stainless steel, 1/2"F x 1" F
	R_4	Reducer, stainless steel, 1/2"M x 1/4"F
	R_HYD_A	Reducer, fluid power (high pressure), 1/2"F x 3/4"M
	R_HYD_B	Reducer, fluid power (high pressure), 1/2"M x 3/4"M
	NM_A	Nipple fitting, stainless steel, 1/2"M
	NM_Z	Nipple fitting, zync, 1/2"M
	NF_Z	Nipple fitting, zync, 1/2"F
	BL_1	Ball valve, 1/2"F
	BL_2	Ball valve, 1/2"F
	TEE_A	Tee junction, stainless steel, 1/2"F
	TEE_B	Tee junction, brass, 1/2"F
	TEE_Z	Tee junction, zync, 1/2"F
	FILTER	Filter Y, brass, 1/2"F

Figure 3. Circuit schematic with fitting definitions and locations

2.1. *Electric Motor*

The electric motor under investigation is the GVM (Global Vehicle Motor) 210 – 300 DPW, engineered, manufactured and sold by Parker Hannifin. The GVM series consists of high-performance permanent magnet synchronous motors specifically engineered for EV propulsion applications. Its main performance specifications are listed below:

- rated power: 155 kW; peak power: 277.8 kW;
- rated torque: 205 Nm; peak torque: 530 Nm;
- rated speed: 7220 rev/min; maximum speed: 8000 rev/min.

The motor is equipped with a liquid cooling circuit and can be cooled using water–glycol mixtures at different concentrations or, alternatively, oil, although motor performance is significantly reduced in the latter case. As specified in the provided datasheet, the maximum coolant temperature and pressure at the motor inlet must not exceed 65 °C and 5 bar, respectively. Furthermore, the maximum allowable coolant temperature rise between inlet and outlet is 10 °C. Since the GVM 210–300 DPW operates with an efficiency higher than 92% over most of its operating range, a coolant flow rate of approximately 20 L/min can be considered sufficient to ensure compliance with these operating limits.

2.2. *Inverter*

The inverter installed in the test-rig is the Parker GVI H650, a high-performance traction inverter designed to supply the electric motor described above. It converts the DC voltage provided by the battery into a controlled three-phase AC voltage, enabling motor speed regulation, torque control, and regenerative braking energy recovery. Its main specifications, reported in the provided datasheet, are reported below:

- nominal voltage: 650 V;
- peak current: 500 A_{rms};
- peak power: 300 kVA..

The inverter is equipped with an internal liquid cooling circuit and is compatible with water–ethylene glycol mixtures at different concentration ratios. According to the datasheet, the coolant temperature and pressure at the inverter inlet must not exceed 60 °C and 2 bar, respectively. In addition, the maximum allowable coolant temperature rise between inlet and outlet is 5 °C.

2.3. *E-Pump*

A prototype screw-type positive-displacement electric pump, provided by the project partner Fluid-o-Tech (FoT), was used [12], [13], [14]. The pump has a volumetric displacement of 13.14 cm^3/rev and integrates an electric motor driven by an inverter supplied at 12 V, with a maximum current absorption of 50 A. The pump is controlled through a speed feedback loop, with the target rotational speed set via dedicated software. The main performance limits of the pump are:

- rotational speed: 6000 rev/min;
- flow rate: 50 L/min;

- pressure difference: 3.2 bar.

The performance curves of the electric pump were provided by the manufacturer and are shown in Figure 4.

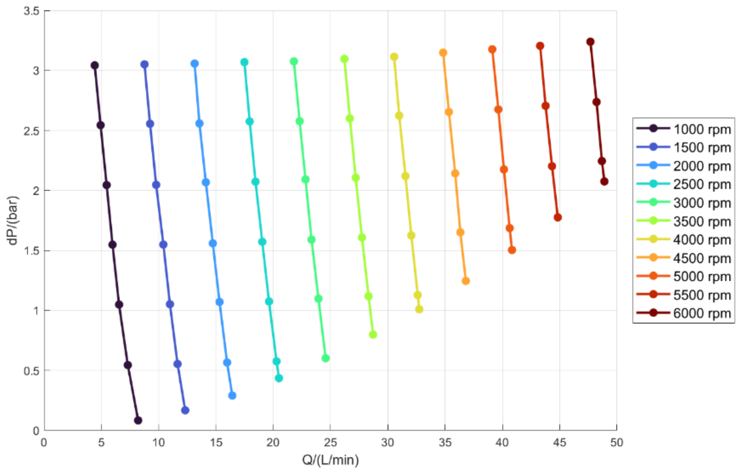

Figure 4. Pump performance curves.

2.4. Fan Coils

The two fan coil units referred to as "Carisma_HEX" and "Aermec_HEX" in Figure 3 respectively represents the selected fan coil units "Carisma CRC44" produced by Sabiana and "FCZ350PO" manufactured by Aermec. Their arrangement in parallel and its series connection with the circuit were adopted to ensure proper heat dissipation while avoiding excessive circuit pressure losses.

3. Numerical Model

The aim of the modelling activity was to reproduce the experimental test-rig using a one-dimensional lumped-parameter approach in the Simcenter AMESim environment. The data obtained from the experimental characterization of the individual components were implemented in the model, and the resulting model was subsequently validated against the experimental measurements. Once validated, the model could support future thermal analyses, which were not performed experimentally since all tests were carried out to hydraulically test components without thermal loading. An overview of the model is presented in Figure 5.

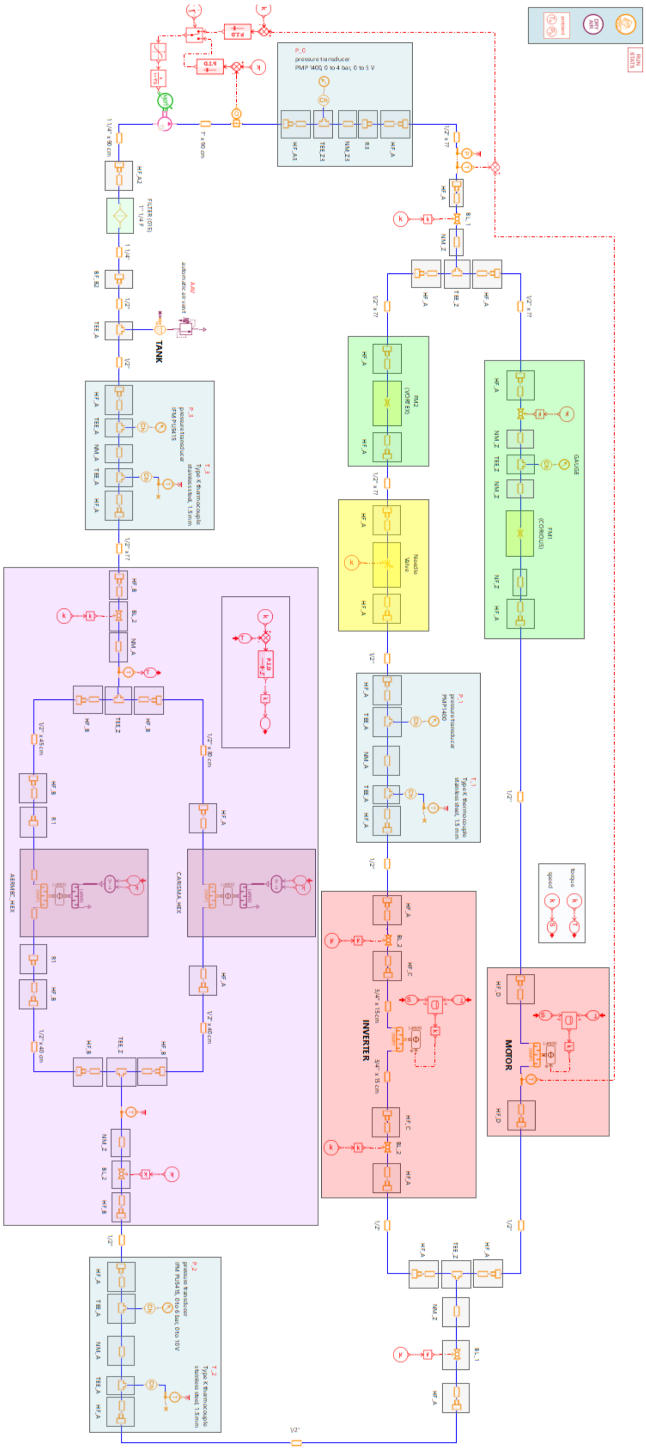

Figure 5. Numerical model of the test-rig reproduced.

3.1. Tank and E-Pump

The system reservoir is modelled as a thermo-hydraulic accumulator, in which the liquid volume is coupled with a pneumatic volume. Air release is reproduced by means of an overpressure valve.

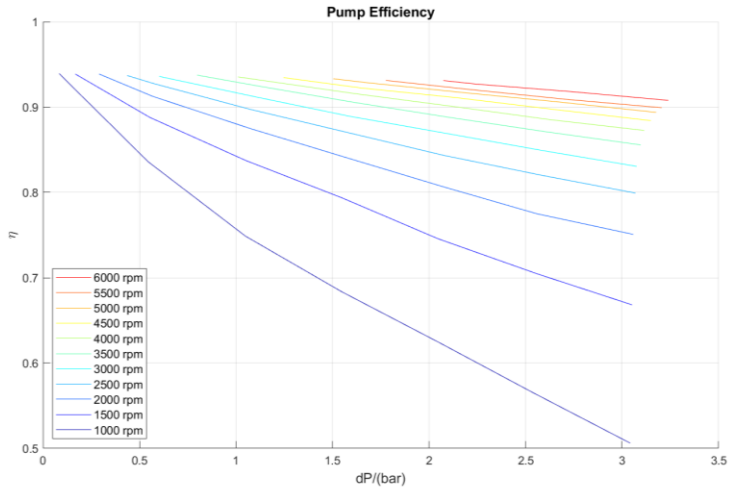

Figure 6. FoT screw pump's efficiency characteristics implemented in the model

The pumping unit is modelled to reproduce the prototypal Fluid-o-Tech positive-displacement pump, with a displacement of 13.14 cm³/rev. The pump efficiency curves implemented in the software are shown in Figure 6. The pump rotational speed is regulated by two separate PID controllers associated with a switching logic based on the simulation time. During the initial phase, the pump speed is regulated according to the error between the flow rate measured by the sensor and the reference value imposed by the user. Once the initialization phase is completed, the control is transferred to the thermal-management PID controller, which adjusts the pump speed to maintain a temperature difference of 10 °C between the inlet and outlet of the electric motor.

The theoretical volumetric flow rate of the pump is given by equation (1), where V is the pump displacement (13.14 cm³/rev) and ω is the shaft speed. The real delivered flow rate is obtained from the volumetric efficiency shown in Figure 6, according to equation (2):

$$Q_{th} = V \cdot \omega \tag{1}$$

$$Q_{real} = Q_{th} \cdot \eta_{vol} \tag{2}$$

As shown in Figure 6, the pump volumetric efficiency drops markedly at the lowest tested rotational speed (1000 rev/min). This behaviour is consistent with the operating principle of a fixed-displacement positive-displacement pump, whose volumetric efficiency is governed by internal leakage flow, which is largely independent of shaft speed. Since the theoretical flow rate is proportional to speed while the leakage flow is not, the leakage represents a progressively larger fraction of the theoretical flow as speed decreases, and this effect is further amplified at high pressure differentials. It should be noted that, within the range of operating conditions investigated experimentally, the combination of 1000 rev/min and high-pressure differential that would be required to fully expose this efficiency drop was not actually reached; the maximum pressure differential recorded at 1000 rev/min remained well below the level associated with the steepest efficiency reduction.

3.2. Motor and Inverter

The electric motor (Parker GVM210–300) and inverter (Parker GVI-H650) are integrated into the numerical model as simplified heat exchangers. The pressure losses in these two components are implemented through Q = f(dP) curves (Figure 7), derived from processed experimental data collected during the flushing tests conducted in the CeSMA/UniNA laboratories.

The heat exchange in these components is modelled by means of a thermal-hydraulic capacitive element, whose thermodynamic state is obtained from the mass and energy balances of the half-heat-exchanger submodel:

$$\frac{dm}{dt} = dm_1 + dm_2 \tag{3}$$

$$\frac{d(mu)}{dt} = dmh_1 + dmh_2 + \dot{Q} \tag{4}$$

where m is the mass and u is the internal energy in the capacity, dm_1, dm_2 and dmh_1, dmh_2 are the mass and enthalpy flow rates at the two hydraulic ports, and $\dot{Q}$ is the heat flux exchanged with the outside, imposed at the opposite side of the element.

In the current configuration, the imposed thermal load can either be set to zero or defined according to one operating point of the electric motor reported in its datasheet.

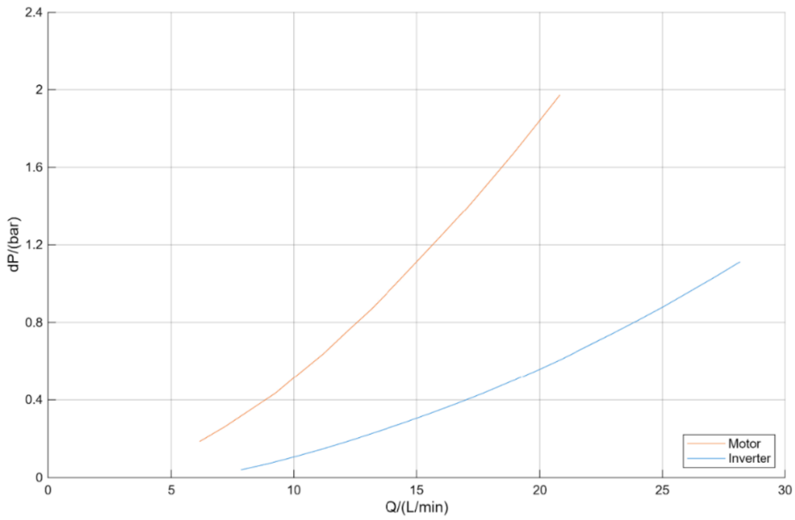

Figure 7. Q = f(dP) curves implemented for motor and inverter (from experimental data)

3.3. Fan Coil Units

The two fan coil units, namely Carisma and Aermec, were implemented in the model as simplified heat exchangers. Each unit consists of two half-heater elements connected through a thermal exchange block, which evaluates the heat transfer between air (cold side) and the coolant (hot side) using the same mass and energy balance formulation described in section 3.2. The air flow rate in the cold side of both heat exchangers is controlled by a PID controller, whose error signal is defined as the difference between the coolant temperature measured downstream of the parallel fan coil connection and the reference value of 25 °C. The pressure drops of the two units are implemented through Q = f(dP) curves, obtained from experimental data and shown in Figure 7.

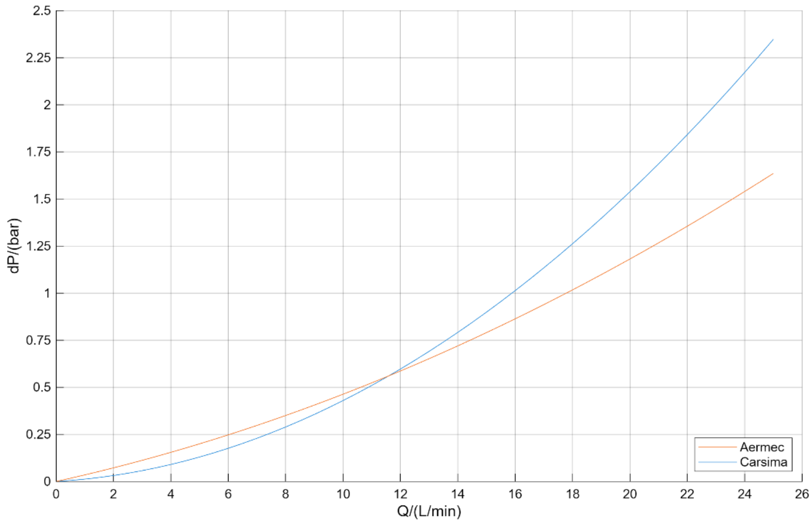

Figure 8. Q = f(dP) curves implemented for Carisma and Aermec (from experimental data)

4. RESULTS AND MODEL VALIDATION

As previously described, the test rig is equipped with a needle valve to regulate the flow distribution between the inverter and motor branches. The valve installed in the experimental setup is the Nieruf NV010003 needle valve. To evaluate the hydraulic behaviour of the system under different flow-splitting conditions, several tests were repeated by varying the valve opening from fully open, corresponding to position 0, to fully closed, corresponding to position 11.5. Each position increment corresponds to one complete turn of the needle valve, up to its complete closure.

As shown in Figure 9 and Figure 10, the flow rate distribution between the two parallel branches, namely the motor branch and the inverter branch, is only slightly affected by the needle valve opening up to position 5. Beyond this threshold, the distribution becomes significantly more uneven, with a marked reduction in the flow rate through the inverter branch. As expected, the total flow rate through the two parallel branches increases with pump rotational speed.

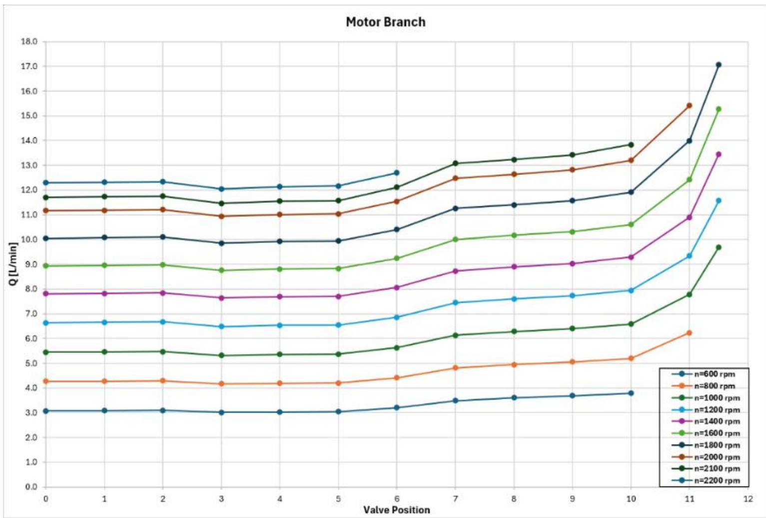

Figure 9. Measured flowrate as function of needle valve opening in the motor branch.

The needle valve was implemented in the model as a variable-section orifice, modelled according to the *Kv* coefficient of 0.66 reported in the datasheet. However, since the physical valve was manually adjusted during the experimental tests, a calibration procedure was required to correlate each experimental valve position with the corresponding control signal of the variable orifice.

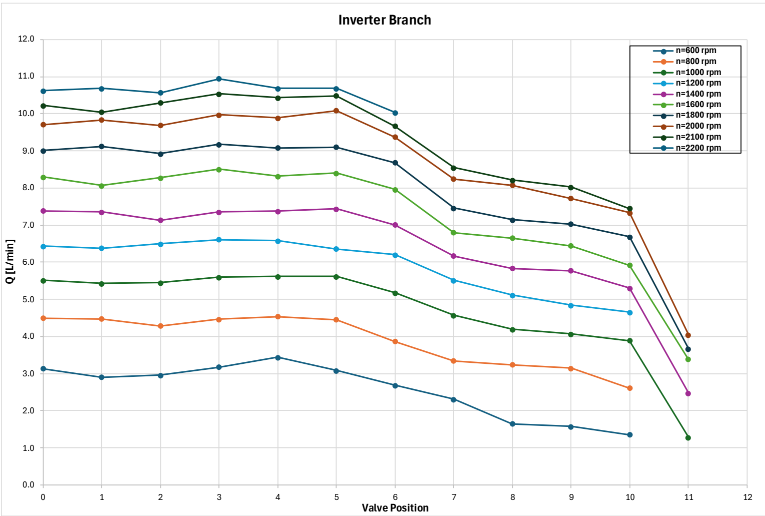

Figure 10. Measured flowrate as function of needle valve opening in the inverter branch.

Since the variable orifice used to represent the physical needle valve does not directly reproduce its mechanical actuation law, an inverse approach was adopted to map each experimental valve position to an equivalent input signal. This mapping was obtained by iteratively adjusting the orifice control signal until the simulated flow distribution between the two parallel branches matched the experimental measurements. During this procedure, the PID controller regulating the pump speed was used to impose the same total flow rate measured during the experimental tests, calculated as the sum of the flow rates through the two parallel branches.

As shown in Figure 11. and Figure 12., after calibration, the model accurately reproduces the flow rate distribution between the two parallel branches over the investigated operating range. The calibration procedure was carried out and validated for all tested valve positions; however, for brevity, only the results corresponding to position 10 are reported here, selected as a representative example.

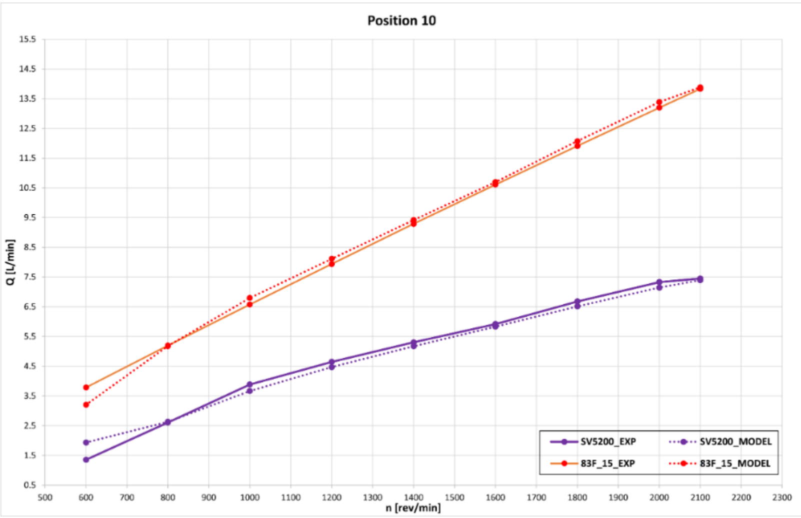

Figure 11. Numerical vs Experimental flowrates comparison with valve position 10.

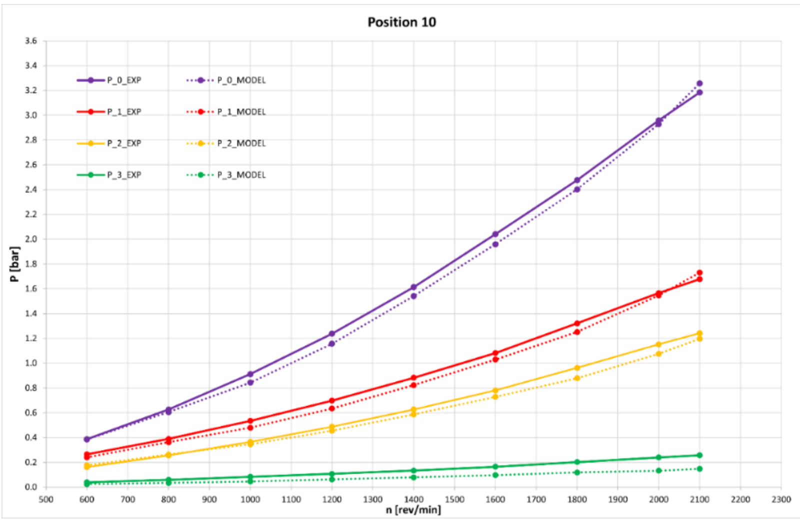

Figure 12. Numerical vs Experimental pressure drops comparison with valve position 10.

A slight divergence between the numerical and experimental flow rates can be observed at the lowest tested pump speed (600 rev/min). This discrepancy is mainly attributed to the pressure-loss characteristics implemented in the model for the pipe fittings, which tend to overestimate local losses at low flow rates compared to their actual behaviour. Since the inverter branch includes a larger number of fittings than the motor branch, this effect is more pronounced on that branch, resulting in a slightly lower simulated flow rate through the inverter branch at the lowest investigated speed.

5. CONCLUSIONS AND FUTURE PERSPECTIVES

This work presents the experimental characterization, numerical modelling, and validation of an innovative thermal management system for a high-performance electric vehicle. The work investigates the use of a prototype positive displacement e-pump as an alternative to conventional solutions that involve centrifugal pumps.

An experimental test rig has been built to replicate the behaviour of a TMS for electric motor and inverter, which have been placed in parallel with respect to the cooling flow, made of a water-glycol mixture (50% vol.). A screw-type e-pump has been tested for water-glycol supply, whose speed is regulated by proprietary software. Flow in the two branches has been regulated using a needle valve. Experimental test-rig measurements confirmed the suitability of the pump for the considered TMS prototype.

A lumped-parameters numerical model has been developed in Simcenter AMESim© environment and validated with experimental data provided by the flow tests, in terms of pressure losses and flow distribution between the motor and the inverter branches. Since variable thermal loads can be imposed on the motor and inverter models, the validated model will support future analyses of the circuit thermo-hydraulic behaviour and enable the comparison of alternative layouts. Future work will also address the pump volumetric efficiency at low rotational speed combined with high pressure differentials, a combination of operating conditions only partially covered by the present experimental campaign.

FUNDING

This research was supported by Italian Ministry of Enterprises and Made in Italy (MIMIT) within the project CLIM (Grant No. F/310129/01-04/X56, CUP B89J23006720005).

6. REFERENCES

[1] L. Chapman, "Transport and climate change: a review," *J. Transp. Geogr.*, vol. 15, no. 5, pp. 354–367, Sep. 2007, doi: 10.1016/J.JTRANGEO.2006.11.008.

[2] J. Sporkmann, Y. Liu, and S. Spinler, "Carbon emissions from European land transportation: A comprehensive analysis," *Transp. Res. D Transp. Environ.*, vol. 121, p. 103851, Aug. 2023, doi: 10.1016/J.TRD.2023.103851.

[3] J. Buberger, A. Kersten, M. Kuder, R. Eckerle, T. Weyh, and T. Thiringer, "Total CO2-equivalent life-cycle emissions from commercially available passenger cars," *Renewable and Sustainable Energy Reviews*, vol. 159, p. 112158, May 2022, doi: 10.1016/J.RSER.2022.112158.

[4] R. B. Gupta, Deveshkumar, and T. Dutta, "Review of Battery Thermal Management Systems for Electric Vehicles," *Lecture Notes in Mechanical Engineering*, pp. 325–335, 2025, doi: 10.1007/978-981-97-7759-4_27.

[5] A. Dhanasekaran *et al.*, "Battery thermal management systems for electric vehicles: A review of current status, opportunities, and future challenges," *J. Energy Storage*, vol. 166, p. 122330, Jul. 2026, doi: 10.1016/J.EST.2026.122330.

[6] G. Previati, G. Mastinu, and M. Gobbi, "Thermal Management of Electrified Vehicles—A Review," *Energies 2022, Vol. 15, Page 1326*, vol. 15, no. 4, p. 1326, Feb. 2022, doi: 10.3390/EN15041326.

[7] H. Jeon, D. Hyun, H. Lee, S. Son, and J. Han, "Optimization of Blades and Impellers for Electric Vehicle Centrifugal Pumps via Numerical Analysis," *Energies 2024, Vol. 17, Page 853*, vol. 17, no. 4, p. 853, Feb. 2024, doi: 10.3390/EN17040853.

[8] A. Petrov and R. L. G. Dias, "Variable speed control in centrifugal pumps for closed systems," *IOP Conf. Ser. Mater. Sci. Eng.*, vol. 963, no. 1, Nov. 2020, doi: 10.1088/1757-899X/963/1/012026.

[9] P. Borriello *et al.*, "A fault detection strategy for an ePump during EOL tests based on a knowledge-based vibroacoustic tool and supervised machine learning classifiers," *Meccanica 2024 59:3*, vol. 59, no. 3, pp. 279–304, Feb. 2024, doi: 10.1007/S11012-024-01754-W.

[10] G. Di Giovine *et al.*, "A Preliminary Design of a Thermal Management System for High-Performance Electric Vehicles: Numerical Simulation and Experimental Validation," *J. Phys. Conf. Ser.*, vol. 3143, no. 1, p. 012068, Dec. 2025, doi: 10.1088/1742-6596/3143/1/012068.

[11] P. Borriello, E. Frosina, P. Lucchesi, and A. Senatore, "Comparative Analysis of Simulation Methodologies for Spindle Pumps," *Fluids 2024, Vol. 9, Page 44*, vol. 9, no. 2, p. 44, Feb. 2024, doi: 10.3390/FLUIDS9020044.

[12] E. Frosina, L. Romagnuolo, S. Li Veli, A. Simeone, C. Roselli, and A. Senatore, "A Preliminary Design of a Thermal Management System for High-Performance Electric Vehicles: Numerical Simulation and Experimental Validation," *J. Phys. Conf. Ser.*, vol. 3143, no. 1, p. 012068, Dec. 2025, doi: 10.1088/1742-6596/3143/1/012068.

[13] P. Borriello, E. Frosina, P. Lucchesi, and A. Senatore, "A Study on a Twin-Screw Pump for Thermal Management Systems by means of CFD using SimericsMP+®: experimental validation and focus on Pressure Pulsation".

[14] P. Borriello, E. Frosina, A. Senatore, and F. Monterosso, "Numerical Modelling and Experimental Validation of Twin-Screw Pumps Based on Computational Fluid Dynamics using SCORG® and SIMERICS MP+®," *E3S Web of Conferences*, vol. 312, Oct. 2021, doi: 10.1051/E3SCONF/202131205007.